ISSN 1068-3755, Surface Engineering and Applied Electrochemistry, 2019, Vol. 55, No. 4, pp. 481–491. © Allerton Press, Inc., 2019.

Inhibitive Effect of 2-[4-(Dimethylamino) Benzylidene] Hydrazinecarbothioamide on Corrosion of Mild Steel in Acidic Solution

Prithvi [a], Preethi Kumari[a], and Suma A Rao[a, *]

[a] *Department of Chemistry, Manipal Institute of Technology, Manipal Academy of Higher Education, Manipal, 576104 India*

**e-mail: suma.rao@manipal.edu*

Received July 6, 2018; revised January 23, 2019; accepted January 25, 2019

Abstract—The inhibition efficiency and adsorption of 2-[4-(dimethylamino) benzylidene] hydrazinecarbothioamide (DABHC) on the corrosion behaviour of mild steel in 0.5M H_3PO_4 and H_2SO_4 solutions has been studied in the temperature range (30–50°C) using potentiodynamic polarization (PDP) and electrochemical impedance spectroscopy (EIS) techniques. The inhibition effectiveness of DABHC increases with increase in its concentration and decreases with increase in temperature. The results indicate that DABHC functions as a mixed type inhibitor and followed Langmuir's adsorption isotherm. The corrosion inhibition of DABHC takes place through physisorption. The surface of the specimen was analysed using scanning electron microscope (SEM) and atomic force microscopy (AFM).

Keywords: mild steel, acid solution, corrosion inhibition, impedance, polarization

DOI: 10.3103/S1068375519040112

INTRODUCTION

Mild steel due to its properties such as tensile strength, hardness and modulus of elasticity together with cast ability, electrical and magnetic properties finds many industrial applications and is one of the most widely used engineering materials. Acid solutions (HCl, H_2SO_4 and H_3PO_4) are often used in industry for cleaning, descaling and pickling processes which are normally accompanied by considerable dissolution of metal [1, 2]. Substantial loss of metal results during acid cleaning and descaling. Hence use of corrosion inhibitors is a very effective and popular method of corrosion control. Studies reveal that synthetic heterocyclic compounds show significant inhibition efficiency due to the presence of N, S, and O [3, 4]. The use of organic compounds and also hydrazide derivatives [5–7] as corrosion inhibitors for mild steel in different acid media has been reported. Literature study reveals that thiosemicarbazide derivatives have been found to be effective in inhibiting corrosion of mild steel to a certain extent in acid solutions [5, 6]. As the continuation of our study of corrosion behaviour of mild steel and combating the same using organic inhibitors [6] we report herein the results of the corrosion inhibition action of 2-[4-(dimethylamino) benzylidene] hydrazinecarbothioamide (DABHC) on mild steel in solutions of H_3PO_4 and H_2SO_4. The corrosion studies are done by potentiodynamic polarization (PDP) and electrochemical impedance methods for 0.5 M acid concentrations both in the absence and with the presence of the DABHC. Further the study includes calculation of activation and thermodynamic parameters for the adsorption of DABHC and to propose the inhibition mechanism.

EXPERIMENTAL

Material

Mild steel (extruded) having chemical composition (wt %) C (0.16), Si (0.18), Mn (0.41), P (0.03), S (0.04), Cr (0.02), Ni (0.02), Mo (0.01), Al (0.004), Cu (0.07) and Fe (remaining) was used for the corrosion study. The test coupons were embedded using cold setting resin. The exposed flat surface (1 cm^2) of the mounted part was polished using emery papers of different grit level and later disc polished using levigated alumina. The polished specimen was washed with double distilled water, rinsed with acetone and dried before immersing in the corrosive medium.

Medium

The stock solution of 2 M H_3PO_4 and H_2SO_4 were prepared from AR grade H_3PO_4 and H_2SO_4 and double distilled water. From the stock solution acids of required strength were prepared as and when required.

Synthesis of DABHC

DABHC was synthesized as per the procedure reported in literature [8]. An equimolar mixture of 4-(dimethylamino) benzaldehyde (0.01 mol) and hydrazinecarbothioamide (0.01 mol) dissolved in ethanol, was kept in a round-bottomed flask. The reaction mixture was refluxed for about 3h on a hot water bath. The precipitated product was filtered, dried, recrystallized from ethanol and characterized using FTIR spectrophotometer (Schimadzu FTIR 8400S) in the frequency range of 4000 to 400 cm^{-1} using KBr pellets The synthetic route for the preparation of DABHC is given in Scheme 1.

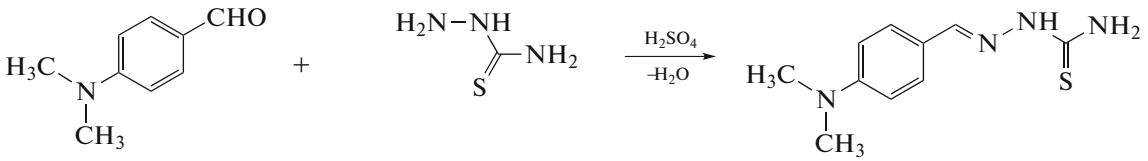

4-(Dimethylamino)benzaldehyde Hydrazinecarbothioamide (2*E*)-2-[4-(dimethylamino)benzylidene]hydrazinecarbothioamide

Scheme 1. Synthetic route for the preparation of DABHC.

Characterization of DABHC

DABHC is a white crystalline solid (95%): $C_{10}H_{14}N_4S$: IR (KBr), cm^{-1}: 3433, 3400 (NH_2 *str.*), 3147 (NH *str.*), 3100 (Ar CH *str.*), 1600 (C=N *str.*) 1504 (Ar C=C *str.*).

Electrochemical measurements

Electrochemical measurements were done using an electrochemical work station 604D series with beta software and a conventional three-electrode Pyrex glass cell with platinum as counter electrode, saturated calomel electrode as reference electrode and mild steel specimen as working electrode.

Polished mild steel test coupon was exposed to 100 mL of the corrosion medium of 0.5 M phosphoric and sulphuric acid solutions without and with various concentrations of DABHC at different temperatures (30–50°C) and steady state open circuit potential (OCP) was noted. The impedance experiments were carried out by applying small amplitude AC signal of 10 mV in the frequency range of 100 kHz to 0.01 Hz, at the OCP. Impedance data were evaluated using Nyquist plots. The current vs. potential curves were recorded by polarizing the test coupon from −250 mV cathodic to +250 mV anodic with respect to the OCP at a scan rate of 0.1 mV s^{-1} and from the plot E_{corr} and i_{corr} values were determined.

Surface Characterization

The SEM and AFM images were recorded for the mild steel specimen corroded in each of 0.5 M phosphoric acid and sulphuric acid solutions both with and without DABHC using scanning electron microscope (EVO 18-5-57 model) and atomic force microscopy (AFM-1B342 Innova model) techniques.

RESULTS AND DISCUSSION

Potentiodynamic Polarization Studies

Potentiodynamic polarization curves for mild steel without and with various concentrations of DABHC in 0.5 M H_3PO_4 and H_2SO_4 solutions at 40°C are shown in Figs. 1a, 1b respectively. Similar plots were recorded at other temperatures in both the acid concentrations. The values of corrosion current density (i_{corr}), corrosion potential (E_{corr}), corrosion rate (*CR*), anodic Tafel slope (β_a), and cathodic Tafel slope (β_c) are recorded in Table 1.

The *CR* is calculated using Eq. (1).

$$CR = \frac{3270 M i_{corr}}{\rho Z}, \quad (1)$$

where the constant 3270 represents the unit, i_{corr} = corrosion current density in A cm^{-2}, ρ = density of the corroding material, *M* = atomic mass of the metal, and *Z* = number of electrons transferred per metal atom [9].

Using the following Eq. (2), percentage inhibition efficiency (*IE* (%)) of the inhibitor was determined.

$$IE(\%) = \frac{i_{corr} - i_{corr(inh)}}{i_{corr}} \times 100, \quad (2)$$

where, i_{corr} and $i_{corr(inh)}$ signify the corrosion current density without and with inhibitor respectively. The surface coverage (θ) is related to percentage inhibition efficiency as follows,

$$\theta = \frac{IE(\%)}{100}. \quad (3)$$

From Table 1 it is evident that the *CR* of mild steel in the absence of DABHC increased with increase in temperature in both the acid solutions. The addition of DABHC brought down the corrosion current and hence corrosion rate. Further the inhibition efficiency

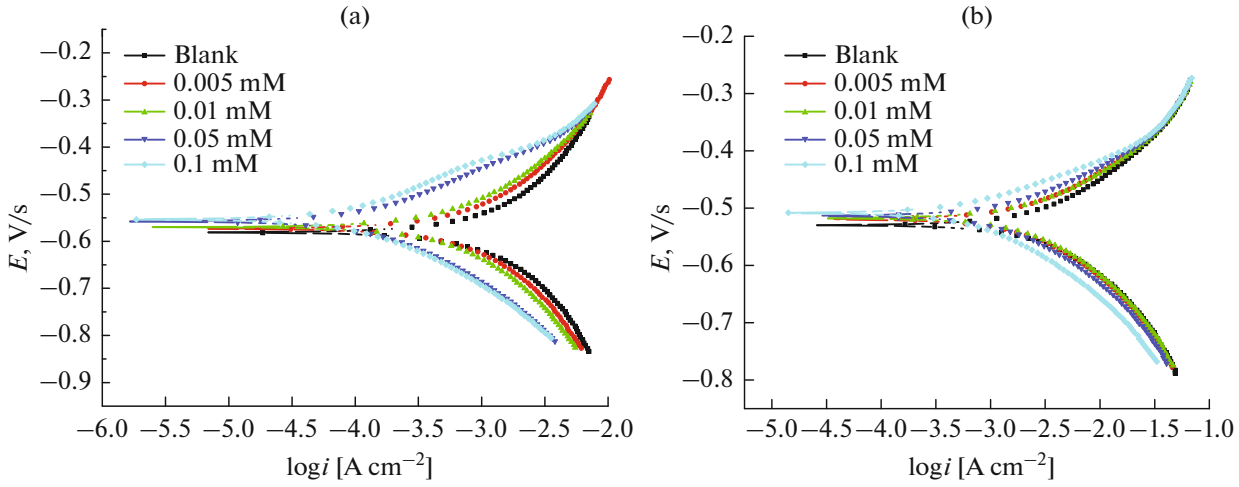

Fig. 1. Potentiodynamic polarization curves for the corrosion of mild steel in (a) 0.5 M H_3PO_4 and (b) 0.5 M H_2SO_4 M containing various concentrations of DABHC at 40°C.

of DABHC increased with increase in its concentration. Decrease in the *CR* may be due to the interaction of the adsorbed inhibitor with surface metal atoms, thus isolating the metal surface from the aggressive medium by simple blocking effect [10]. If the decrease in *CR* is due only to hydrogen overvoltage (or complex formation) the decrease should almost remain constant (acid strength is 0.5 M) irrespective of concentration of the inhibitor which is not the case.

DABHC showed maximum inhibition efficiency of 85% in 0.5 M H_3PO_4 and around 75% in 0.5 M H_2SO_4 at 30°C. The obtained result is similar to the inhibition efficiency reported in the study of corrosion inhibition of mild steel in HCl medium using (2E)-2-(3-hydroxy-2-methoxybenzilidene) hydrazinecarbothiamide obtained in the range of 68 to 90% and around 80 to 90% in case of 2-(3,4,5-trimethoxy benzylidene) hydrazine carbothioamide [5, 6].

It is evident from the polarization plots that the presence of DABHC showed a positive shift in E_{corr} value. It is reported [11] that if the shift in corrosion potential exceeds ±85 mV with respect to corrosion

Table 1. Potentiodynamic polarization results for the corrosion of mild steel in 0.5 M H_3PO_4 and 0.5 M H_2SO_4 in the absence and presence of DABHC at different temperatures

Temp., °C	DABHC, mM	0.5 M H_3PO_4			0.5 M H_2SO_4		
		i_{corr}, mA cm^{-2}	*CR*, mpy	*IE*, %	i_{corr}, mA cm^{-2}	*CR*, mpy	*IE*, %
30	0	0.917	213.3	–	1.860	432.5	–
	0.005	0.532	121.9	42.8	1.337	311.0	28.1
	0.01	0.311	72.54	65.9	1.260	293	32.2
	0.05	0.122	28.48	86.6	0.668	155.5	64.0
	0.1	0.076	17.78	91.6	0.374	87.09	79.6
40	0	1.287	299.3	–	2.953	686.9	–
	0.005	0.973	226.4	24.3	2.30	535.0	22.1
	0.01	0.521	121.2	59.4	2.103	530.0	28.7
	0.05	0.259	60.46	79.8	1.456	338.8	50.6
	0.1	0.106	24.75	91.0	0.664	154.4	77.5
50	0	1.757	408.6	–	4.397	1023	–
	0.005	1.501	349.1	14.5	4.308	1019	6.7
	0.01	1.374	319.6	21.7	3.956	920.2	10.2
	0.05	0.808	188.1	53.9	3.402	795.4	22.6
	0.1	0.207	48.35	88.1	2.053	477.6	53.3

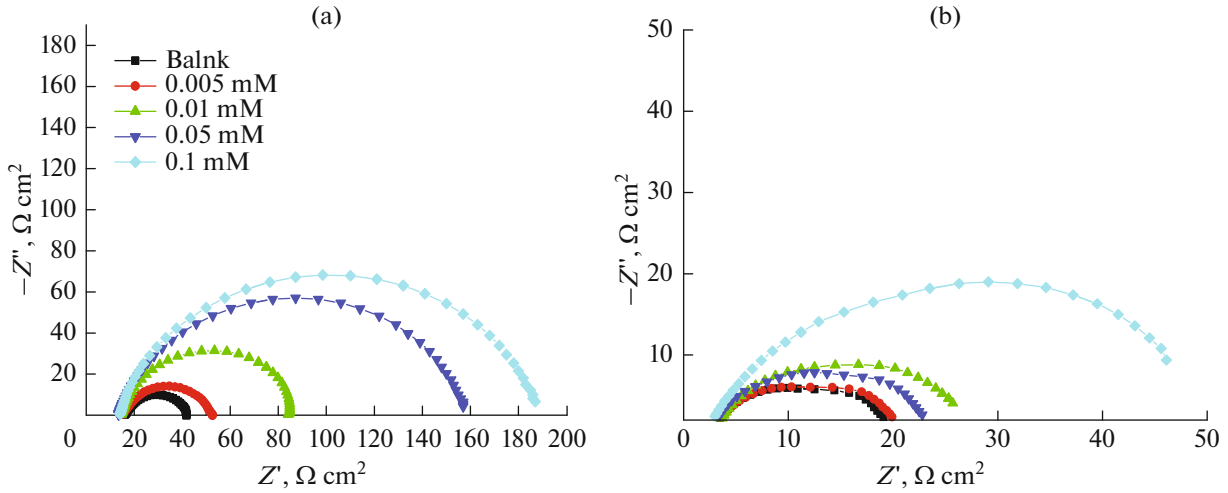

Fig. 2. Nyquist plots for corrosion of mild steel in (a) 0.5 M H_3PO_4 acid and (b) 0.5 M H_2SO_4 acid containing different concentrations of DABHC at 40°C.

potential of the uninhibited solution, the inhibitor acts as either anodic or cathodic type. In the present case the maximum displacement in E_{corr} is found to be within +20 mV, which indicates that present inhibitor acts as mixed type of inhibitor by showing its inhibitory action on both hydrogen evolution and metal dissolution. Further it is seen that anodic polarization curves did not exhibit linear ehavior in 0.5 M H_3PO_4 and the cathodic polarization curves showed linear behavior. Anodic polarization curves showed the inflection points at potentials more positive than corrosion potential (E_{corr}), characterized by two different slopes indicating a kinetic barrier effect, possibly due to the deposition of a surface film followed by its dissolution at increased anodic potential [12]. Values of cathodic slope (b_c) did not vary significantly with increase in inhibitor concentration, which indicates that the hydrogen evolution is activation-controlled and the presence of inhibitor does not alter the inhibition mechanism [13].

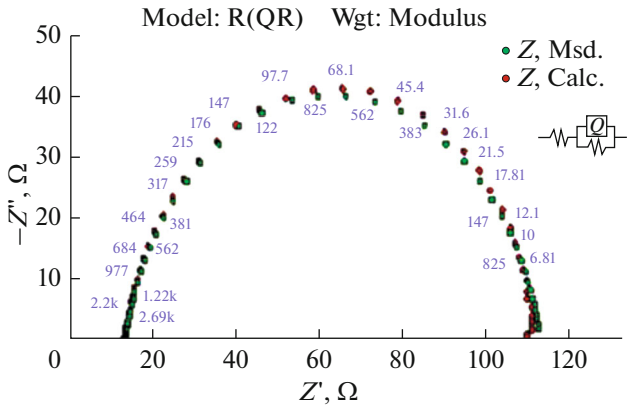

Fig. 3. Equivalent circuit used fit the impedance parameters without and with DABHC.

Electrochemical Impedance Spectroscopy Studies

The Nyquist plots for the corrosion behaviour of mild steel without and with DABHC in 0.5 M H_3PO_4 and H_2SO_4 at 40°C are given in Figs. 2a, 2b respectively. In the plots obtained with depressed semicircle it is observed that the diameter increased with increase in inhibitor concentration, suggesting that the charge transfer process is mainly controlling the corrosion of mild steel. The contribution from roughness of the surface, active sites distribution or inhibitor adsorption can be credited to the depressed capacitive behaviour.

The impedance parameters were analysed using ZSimpWin software version 3.21 by fitting suitable equivalent circuit to the Nyquist plots. A simplest Randle's equivalent circuit as shown in Fig. 3 was used to fit the Nyquist plot without and with inhibitor in both acid solutions. It consists of solution resistance R_s, charge transfer resistance R_{ct} and one constant phase element (*CPE*). *CPE* was employed instead of the double-layer capacitance C_{dl} to describe the heterogeneity in the system [14]. The impedance parameters obtained are reported in Table 2.

The *CPE* behaves like an ideal double-layer capacitance (C_{dl}) and was calculated from the frequency (f_{max}) at which the imaginary component of impedance was maximum ($Z_{imp,max}$) using the following equation,

$$C_{dl} = \frac{1}{2\pi R_{ct} f_{max}}. \quad (4)$$

Due to the replacement of the adsorbed water molecule from the metal surface by the adsorbed inhibitor

Table 2. Results of EIS measurements for the corrosion of mild steel in 0.5 H_3PO_4 and 0.5M H_2SO_4 in the absence and presence of DABHC at different temperatures

Temp., °C	DABHC, mM	0.5 M H_3PO_4			0.5 M H_2SO_4		
		C_{dl}, μF cm^{-2}	R_{ct}, Ω cm^2	*IE*, %	C_{dl}, μF cm^{-2}	R_{ct}, Ω cm^2	*IE*, %
30	0	676	23.74	–	1096	14.63	–
	0.005	265	43.0	44.7	719	15.13	27.1
	0.01	63.8	80.0	70.3	557	18.89	30.5
	0.05	18.8	150	84.1	394	21.39	63.2
	0.1	11.8	199	88.0	96.7	40.58	78.0
40	0	1889	13.54	–	3338	7.42	–
	0.005	900	18.42	26.4	1547	10.45	20.5
	0.01	239	31.98	57.6	702	10.96	25.7
	0.05	49.2	78.90	82.8	334	11.54	49.5
	0.1	22.3	128.3	89.4	163	17.45	75.5
50	0	3353	12.81	–	6076	5.043	–
	0.005	2103	14.57	12.0	5223	5.696	2.0
	0.01	1227	16.90	24.2	5099	5.787	9.5
	0.05	405	21.52	40.4	1359	6.374	22.5
	0.1	57.1	83.54	84.6	613	7.008	50.6

molecules, the increase in inhibitor concentration tends to decrease the double layer capacitance (C_{dl}). Further the decrease in C_{dl} was attributed to increase in the thickness of the electrical double layer at the metal/solution interface [15]. The charge transfer resistance R_{ct} is a measure of resistance against electron transfer across the surface and is inversely proportional to *CR*.

$$IE\,(\%) = \frac{R_{ct(inh)} - R_{ct}}{R_{ct(inh)}}, \qquad (5)$$

where R_{ct} and $R_{ct(inh)}$ indicate the charge transfer resistance in presence and absence of inhibitor. The increase in charge transfer resistance R_{ct} increases with increase in inhibitor concentration indicates that the corrosion process is mainly controlled by the charge transfer process [4]. This also suggests that the amount of the inhibitor molecules adsorbed on to the metal surface increases as the concentration of inhibitor molecule increases. The adsorbed inhibitor molecules subsequently result in the formation of a barrier film on the metal surface thereby reducing the *CR*.

Effect of Temperature

The influence of temperature on *CR* was studied in the temperature range 30 to 50°C at different concentrations of DABHC. It can be seen from Table 1 that the inhibition efficiency decreased with increase in temperature. This may be due to desorption of the adsorbed inhibitor molecules from the metal surface with increase in temperature [12, 13]. This suggests physisorption. Arrhenius equation (Eq. (6)) was used to calculate the activation energy (E_a) for the corrosion process.

$$\ln(CR) = B - \frac{E_a}{RT}, \qquad (6)$$

where *B* is the Arrhenius pre-exponential constant, and *R* is the universal gas constant.

Neglecting the temperature dependency of the pre exponential term *B*, Arrhenius plot ln*CR* vs $1/T$ for corrosion of mild steel in 0.5 M H_3PO_4 and H_2SO_4 are shown in Figs. 4a, 4b.

The slope obtained from the plot of ln *CR* vs $1/T$ was used to calculate the effective activation energy for the corrosion and inhibition process [12]. The thermodynamic properties for the metal dissolution process which is dependent on rate determination step were determined using transition state Eq. (7).

$$CR = \frac{RT}{Nh}\exp\left(\frac{\Delta S^{\#}}{RT}\right)\exp\left(\frac{-\Delta H^{\#}}{RT}\right), \qquad (7)$$

where *h* is Planck's constant and *N* is Avogadro's number [16]. Plot of ln (CR/T) vs $1/T$ (Figs. 5a, 5b), gave a straight line with slope $-\Delta H^{\#}/R$ and intercept ln $(R/Nh) + \Delta S^{\#}/R$. The obtained parameters for the corrosion of mild steel in 0.5 M H_3PO_4 and H_2SO_4 are reported in Table 3.

It is observed from Table 3 that in both cases of 0.5 M phosphoric and 0.5 M sulphuric acid there is an increase in the value of activation energy with increase in inhibitor concentration suggesting an increase in

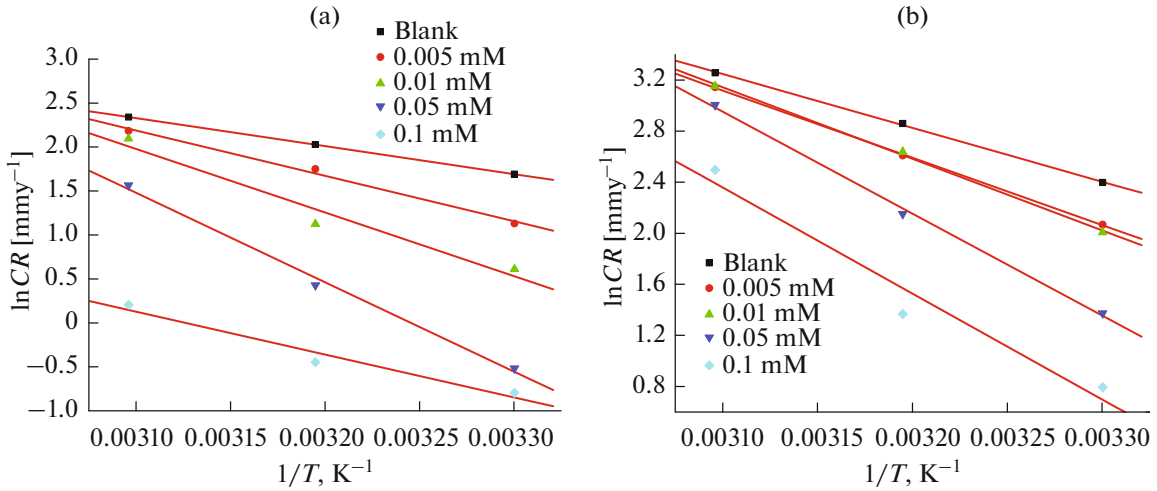

Fig. 4. Plot of ln(*CR*) vs $1/T$ for the mild steel in (a) 0.5 M H_3PO_4 and (b) 0.5 M H_2SO_4 M with various concentration of DABHC.

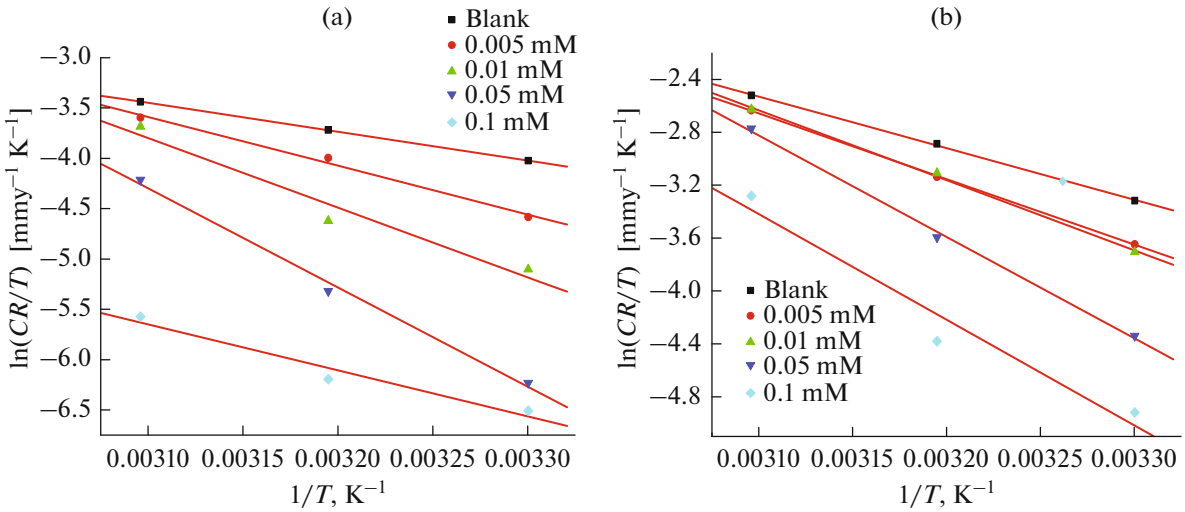

Fig. 5. Plot of ln(*CR*/*T*) vs $1/T$ for the mild steel in (a) 0.5 M H_3PO_4 and (b) 0.5 M H_2SO_4 M with various concentration of DABHC.

energy barrier for the *CR* determination reaction [17]. The negative value of entropy of activation ($\Delta S^{\neq}$) indicates that decrease in disordering takes place on going from reactant to the activated complex and the positive sign of the $\Delta H^{\neq}$ showed the endothermic nature of steel dissolution process [18].

Table 3. Activation parameter for the corrosion of mild steel in 0.5 M H_3PO_4 and 0.5 M H_2SO_4

DABHC, mM	0.5 M H_3PO_4			0.5 M H_2SO_4		
	E_a, kJ mol^{-1}	ΔH, kJ mol^{-1}	$-\Delta S^{\neq}$, J mol^{-1} K^{-1}	E_a, kJ mol^{-1}	$\Delta H^{\neq}$, kJ mol^{-1}	$-\Delta S^{\neq}$, J mol^{-1} K^{-1}
0	19.81	17.21	192.0	35.04	32.44	117.9
0.005	42.87	40.27	186.1	43.81	41.21	91.8
0.01	38.78	58.05	179.8	46.59	43.79	83.4
0.05	36.85	74.01	171.2	66.35	63.74	23.3
0.1	41.31	37.93	189.0	68.97	66.37	20.2

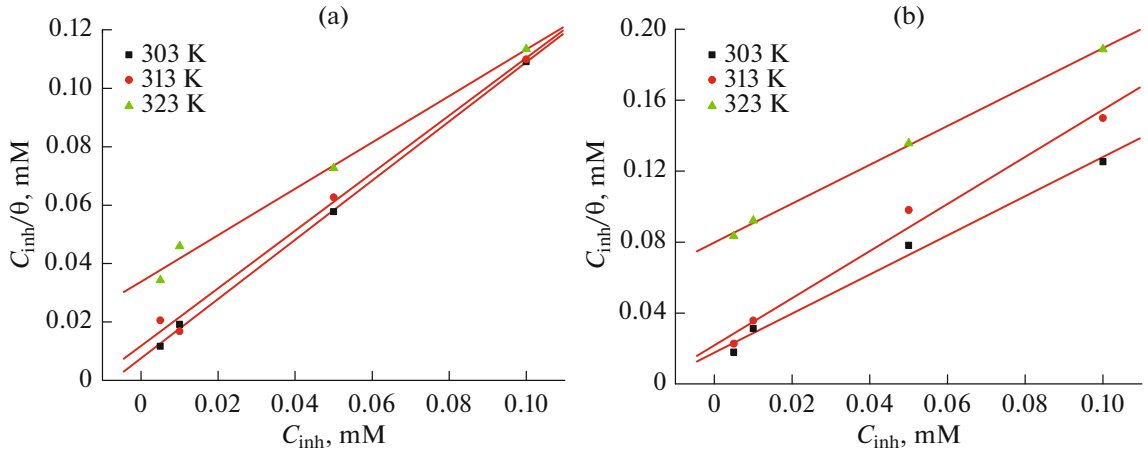

Fig. 6. Langmuir adsorption isotherm of mild steel in (a) 0.5 M H_3PO_4 and (b) 0.5 M H_2SO_4.

Adsorption Considerations

Adsorption isotherm provides information about the interaction between inhibitor and metal surface, which helps to arrive at the corrosion inhibition mechanism. The inhibitor adsorbs on the metal surface and forms a protective film, which acts as barrier between metal surface and corrosive medium. The values of surface coverage (θ) at different concentrations of inhibitor have been used to explain the various isotherms to fit the adsorption process. In the temperature range studied the best correlation between the experimental results and the isotherm function followed Langmuir's adsorption isotherm, which is given by the expression (8)

$$\frac{C_{inh}}{\theta} = \frac{1}{K} + C_{inh}, \quad (8)$$

where K value represents the equilibrium constant for metal–inhibitor interaction, C_{inh} is the inhibitor concentration, and θ is the degree of surface coverage [19].

The plots of (C_{inh}/θ) versus C_{inh} for different temperatures gave straight lines with intercept $1/K$ as shown in Figs. 6a, 6b.

The values of standard free energy of adsorption are related to K by the relation (9) [20].

$$K = \frac{1}{55.5}\exp\left(\frac{-\Delta G^{\circ}_{ads}}{RT}\right), \quad (9)$$

where R is the universal gas constant, T is the absolute temperature, and 55.5 is the concentration of water in solution in mol dm^{-3}. Similarly the plots of ΔG°_{ads} versus T are shown in Figs. 7a, 7b for H_3PO_4 and H_2SO_4 respectively.

The isotherm that best fits the experimental data was chosen using the correlation coefficient (R^2). The correlation coefficient and slope values are found to be very close to unity indicating that the adsorption of DABHC obeyed Langmuir's adsorption isotherm. Generally, the standard free energy values of the order −20 kJ mol^{-1} or less negative are associated with physisorption and −40 kJ mol^{-1} or more negative are associated with chemisorption [21].

It can be seen from Table 4 that the calculated ΔG°_{ads} values are found to be in between 20 and 40 kJ mol^{-1}. This indicates the corrosion inhibition of DABHC is through mixed adsorption predominantly through physisorption. Further the negative values of ΔH°_{ads} confirms the physisorption of DABHC on mild steel in both the acid concentration. The ΔS°_{ads} values are found to be positive, indicating that the increase in disordering takes place on going from the reactant to the adsorbed inhibitor species [22].

Corrosion Inhibition Mechanism

Corrosion inhibition of many metals in acidic solution can be explained based on adsorption phenomenon. The adsorption of inhibitors depends on factors such as the nature of the metal surface, the chemical structure of the organic inhibitor, the distribution of charge in the inhibitor molecule, the nature of electrolyte, and the type of interaction between organic molecules and the metallic surface. In the presence of phosphoric and sulphuric acid medium the mild steel undergoes dissolution and get positive charge on its surface as in galvanic cells. The phosphate ion from the phosphoric acid solution or sulphate ion from sulphuric acid solution get first adsorbed at the metal/solution interface at the corrosion potential through electrostatic attraction force due to the excess positive charge at this interface and changes the charge on the solution side of the interface from positive to negative. This negative charge will attract the protonated DABHC molecules from the acid solution facilitating physisorption of DABHC [23] as shown in

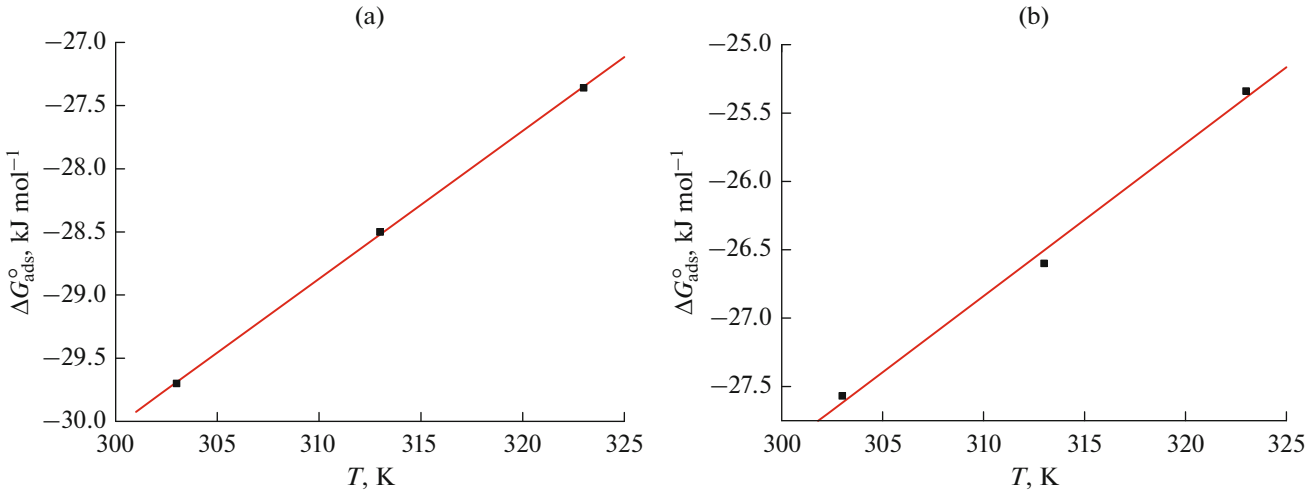

Fig. 7. Plot of ΔG°_{ads} versus T for the adsorption of DABHC on mild steel in 0.5 M H_3PO_4 and 0.5 M H_2SO_4.

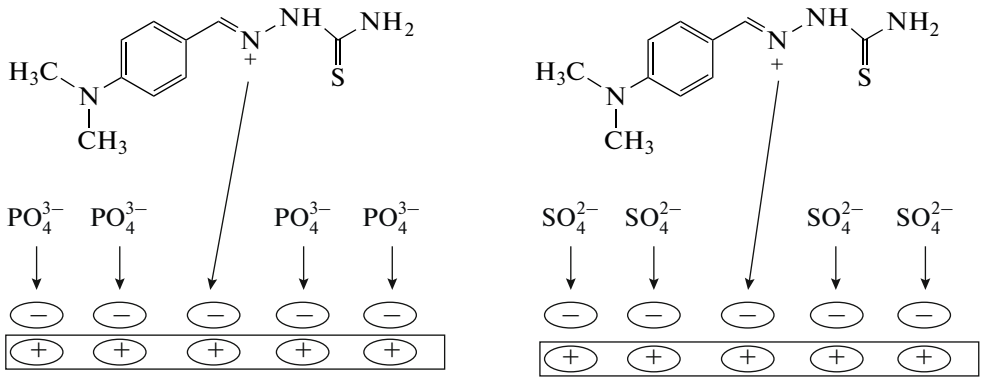

Fig. 8. Adsorption of DABHC on mild steel through electrostatic interaction (physisorption) (a) in 0.5 M H_3PO_4 and (b) in 0.5 M H_2SO_4 medium.

Fig. 8. Furthermore, the protonated inhibitor molecules can also be adsorbed at cathodic sites of metal in competition with hydrogen ions. The adsorption of protonated inhibitor molecules reduces the rate of hydrogen evolution reaction along with metal oxidation resulting in physisorption.

Surface Characterization

The surface characterization of the corroded specimen material was carried out by scanning electron microscopic (SEM) and atomic force microscopic (AFM) studies both in the absence and presence of inhibitor. The SEM and AFM images of the specimen

Table 4. Thermodynamic parameters for the adsorption of DABHC on metal in 0.5 H_3PO_4 and 0.5 M H_2SO_4 at different temperatures

Temp., K	0.5 M H_3PO_4				0.5 M H_2SO_4			
	Slope	$-\Delta G^\circ_{ads}$, kJ mol^{-1}	ΔH°_{ads}, kJ mol^{-1}	ΔS°_{ads}, J mol^{-1} K^{-1}	Slope	$-\Delta G^\circ_{ads}$, kJ mol^{-1}	ΔH°_{ads}, kJ mol^{-1}	ΔS°_{ads}, J mol^{-1} K^{-1}
303	0.999	29.6	−65.4	100.2	0.999	27.5	−61.4	115
313	0.999	29.5			0.999	26.6		
323	0.999	27.3			0.999	25.34		

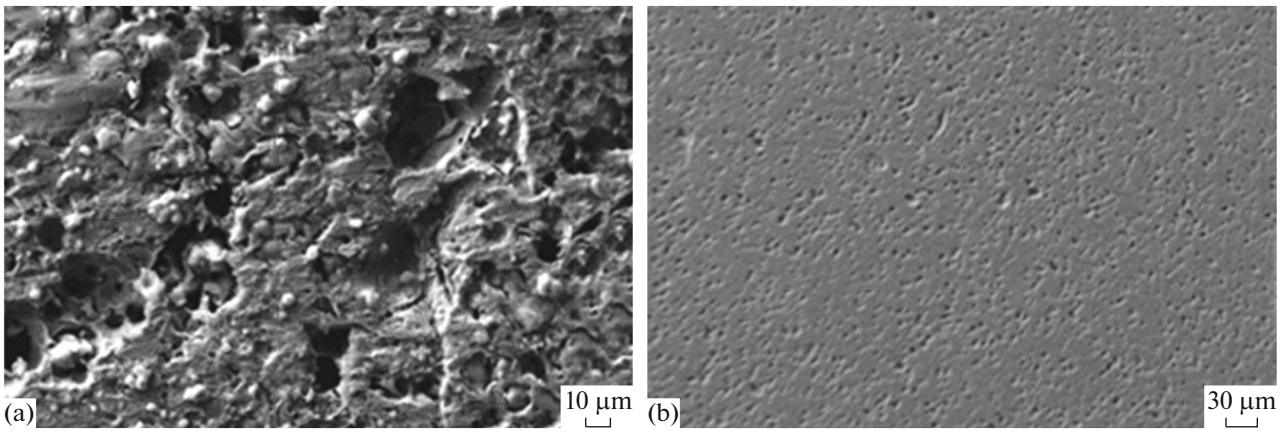

Fig. 9. SEM images of mild steel specimen (a) 0.5 M H_3PO_4 solution, (b) 0.5 M H_3PO_4 solution containing 0.1 mM DABHC.

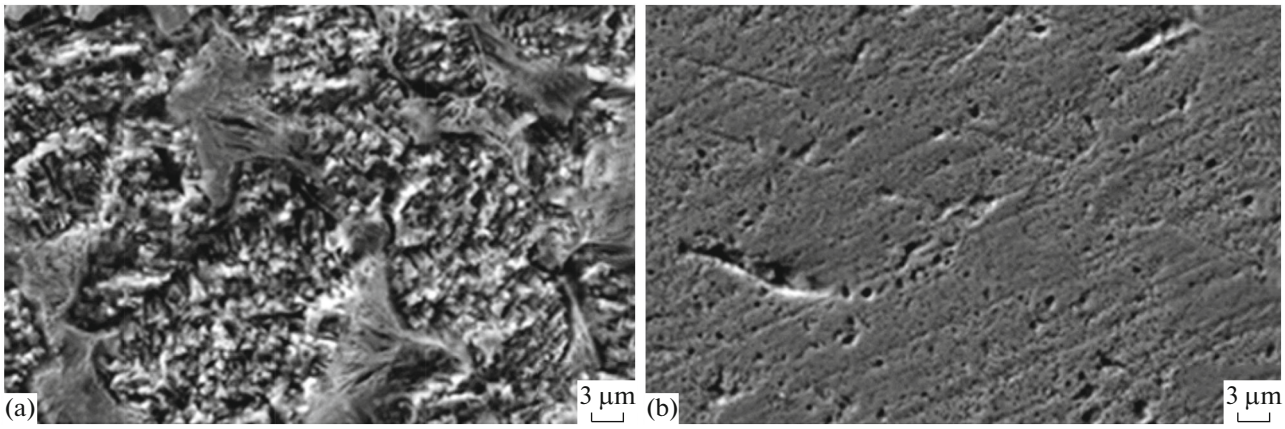

Fig. 10. SEM images of mild steel specimen (a) 0.5 M H_2SO_4 solution, (b) 0.5 M H_2SO_4 solution containing 0.1 mM DABHC.

samples were recorded by subjecting the specimen material to corrosion in 0.5 M H_3PO_4 and 0.5 M H_2SO_4 acid for 3 h in the presence and the absence of DABHC.

Figures 9a, 9b show SEM images of sample in the absence and presence of DABHC in 0.5 M H_3PO_4 acid and Figs. 10a, 10b show SEM images of sample in the absence and presence of DABHC in 0.5 M H_2SO_4 acid.

Figures 9a and 10a show the rough surface and pit formation on the surface of mild steel specimen due to the corrosive action of 0.5 M H_3PO_4 and 0.5 M H_2SO_4 respectively. Figures 9b and 10b showed a smooth sample surface without any visible corrosion attack in the presence of DABHC in 0.5M H_3PO_4 and 0.5 M H_2SO_4 respectively. Figures 11a, 11b and 12a, 12b show 3-dimensional (3D) AFM images of mild steel specimen before and after immersion in 0.5 M H_3PO_4 and 0.5 M H_2SO_4 containing DABHC respectively. The AFM images obtained in the presence of DABHC for both the acid concentration showed a smooth surface in comparison with the AFM images of mild steel specimen in the absence of DABHC. The average surface roughness (R_a) and root-mean-square (RMS) roughness (R_q) values obtained in the absence and presence of DABHC in 0.5 M H_3PO_4 and 0.5 M H_2SO_4 are given in Table 5. The decrease in the R_a and R_q values for DABHC in both the acid medium clearly indicates the decrease in the surface roughness of materials due to adsorption to a certain extent.

Table 5. AFM results obtained for anticorrosive performance of DABHC on mild steel in 0.5 M H_3PO_4 and 0.5 M H_2SO_4

Sample: Mild steel	R_a	R_q
Mild steel + 0.5 M H_3PO_4	458	561
Mild steel + 0.5 M H_3PO_4 + DABHC	250	305
Mild Steel + 0.5 M H_2SO_4	411	519
Mild Steel + 0.5 M H_2SO_4 + DABHC	234	297

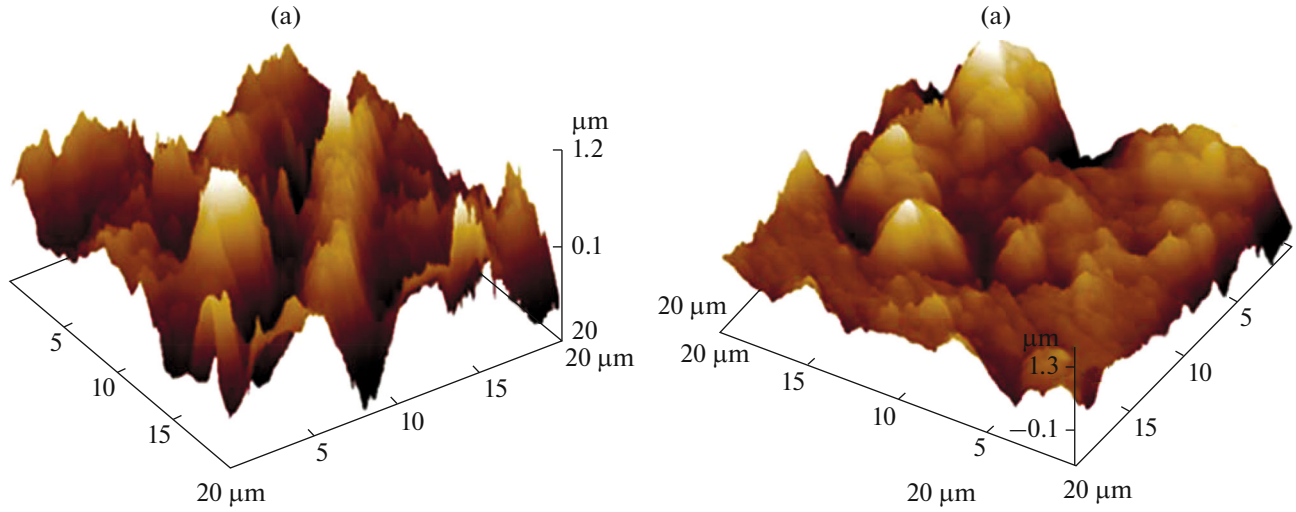

Fig. 11. AFM images of mild steel specimen (a) in 0.5 M H_3PO_4 and (b) 0.5 M H_3PO_4 + DABHC.

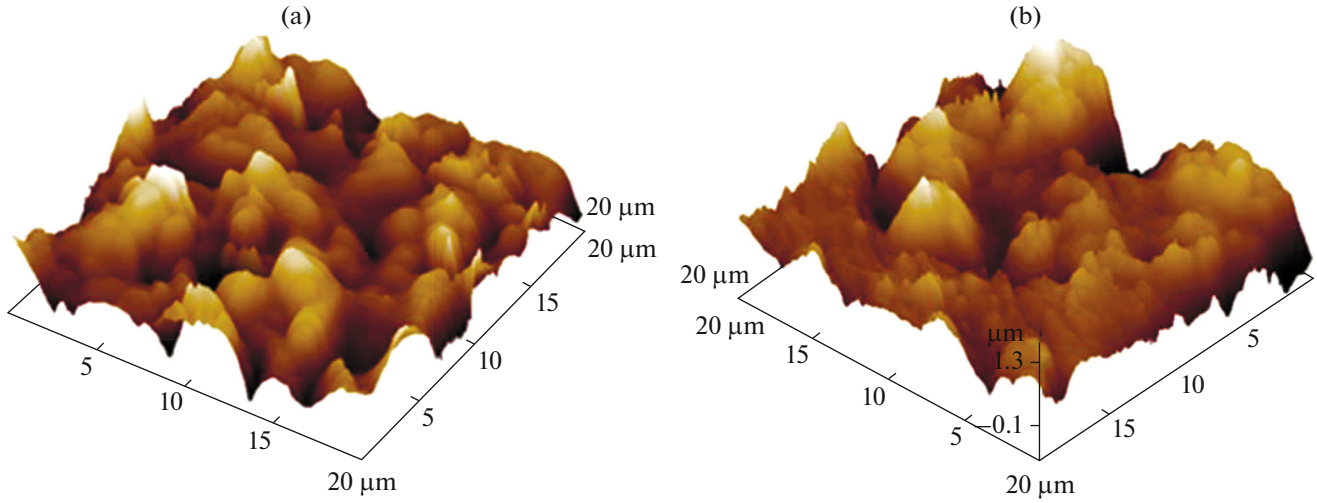

Fig. 12. AFM images of mild steel specimen (a) in 0.5 M H_2SO_4 and (b) 0.5 M H_2SO_4 + DABHC.

CONCLUSIONS

Based on the results of investigation, the following conclusions are drawn:

(1) DABHC inhibit both anodic and cathodic reactions to similar extent, thereby predominantly acting as mixed type of inhibitor.

(2) The inhibition efficiency of DABHC increases with the increase in inhibitor concentrations and decreases with increase in temperatures in both the acid media.

(3) DABHC showed reasonably good inhibition efficiency in phosphoric acid medium when compared to sulphuric acid medium.

(4) The adsorption of DABHC on the metal surface follows Langmuir's adsorption isotherm in both the acid media.

(5) Activation and thermodynamic parameters indicate that the adsorption of DABHC is predominantly through physisorption both in 0.5 M phosphoric and sulphuric acid media.

ACKNOWLEDGMENTS

The authors are grateful to Manipal Institute of Technology and Manipal Academy of Higher Education, Manipal for providing laboratory facilities.

CONFLICT OF INTEREST

The authors declare that they have no conflict of interest.

REFERENCES

1. Prabhu, R.A., Venkatesha, T.V., Shanbhag, A.V., Praveen, B.M., et al., *Mater. Chem. Phys.*, 2008, vol. 108, pp. 283–289.
2. Ezeoke, A.U., Obi-Egbedi, N.O., Adeosun, C.B., and Adeyemi, O.G., *Int. J. Electrochem. Sci.*, 2012, vol. 7, pp. 5339–5355.
3. El-Etre, A.Y., *Mater. Chem. Phys.*, 2008, vol. 108, pp. 278–282.
4. Shetty, P., *Surf. Eng. Appl. Electrochem.*, 2017, vol. 53, pp. 587–591.
5. Preethi Kumari, P., Shetty, P., and Rao, S.A., *Arab. J. Chem.*, 2017, vol. 10, pp. 653–663.
6. Preethi Kumari, P., Shetty, P., Rao, S.A., and Sunil, D., *Rev. Roum. Chim.*, 2014, vol. 59, no. 5, pp. 323–333.
7. Preethi Kumari P., Shetty, P. and Rao, S.A., *Prot. Met. Phys. Chem.*, 2015, vol. 51, pp. 1034–1042.
8. de Oliveira, R.B., de Souza-Fagundes, E.M., Soares, R.P.P., Anderson, A.A., et al., *Eur. J. Med. Chem.*, 2008, vol. 43, pp. 1983–1988.
9. Fontana, M.G., *Corrosion Engineering*, New York: McGraw-Hill, 1987, 3rd ed.
10. Ashish, K. and Sumayah, B., *Int. J. ChemTech Res.*, 2015, vol. 7, pp. 391–396.
11. Li, W., He, Q., Zhang, S., Pei, C., et al., *J. Appl. Electrochem.*, 2008, vol. 38, pp. 289–295.
12. Kumar, P. and Shetty, A.N., *Surf. Eng. Appl. Electrochem.*, 2013, vol. 49, pp. 253–260.
13. Anbarasi, C.M. and Auxilia, A.J., *Int. J. ChemTech Res.*, 2016, vol. 9, pp. 218–225.
14. Barsoukov, E. and Macdonald, J.R., *Impedance Spectroscopy: Theory, Experiment and Applications*, 2nd ed., Hoboken, NJ: Wiley, 2005, p. 13.
15. Tang, Y., Che, Y. and Yang, W., *J. Appl. Electrochem.*, 2008, vol. 38, pp. 1553–1559.
16. Yahalom, J., *Corros. Sci.*, 1972, vol. 12, pp. 867–868.
17. Raja, A.S. and Prathipa, V., *Int. J. ChemTech Res.*, 2015, vol. 8, pp. 134–142.
18. Bentiss, F., Lebrini, M., and Lagrenee, M., *Corros. Sci.*, 2005, vol. 47, pp. 2915–2931.
19. Fekry, A.M. and Ameer, M.A. *Int. J. Hydrogen Energy*, 2010, vol. 35, pp. 7641–7651.
20. Olivares, O., Likhanova, N.V., Gomez, B., Navarrete, J., et al., *Appl. Surf. Sci.*, 2006, vol. 252, pp. 2894–2909.
21. Hosseini, M.S., Mertens, F.L., and Arshadi, M., *Corros. Sci.*, 2003, vol. 45, pp. 1473–1489.
22. Shivakumar, S.S. and Mohana, K.N., *J. Mater. Environ. Sci.*, 2013, vol. 4, pp. 448–459.
23. Elayyachy, M.A., Idrissi, A.E., and Hammouti, I.B., *Corros. Sci.*, 2006, vol. 48, pp. 2470–2479.